Available online at www.sciencedirect.com

ScienceDirect

Journal of Bionic Engineering 8 (2011) 406–417

Numerical Study of Propulsion Mechanism for Oscillating Rigid and Flexible Tuna-Tails

Liang Yang[1], Yumin Su[1], Qing Xiao[2]

1. *State Key Laboratory of Autonomous Underwater Vehicle*, *Harbin Engineering University*, *Harbin* 150001, *P. R. China*

2. *Department of Naval Architecture and Marine Engineering*, *University of Strathclyde*, *Glasgow G*4 0*LZ*, *United Kingdom*

Abstract

Numerical study on the unsteady hydrodynamic characteristics of oscillating rigid and flexible tuna-tails in viscous flow-field is performed. Investigations are conducted using Reynolds-Averaged Navier–Stokes (RANS) equations with a moving adaptive mesh. The effect of swimming speed, flapping amplitude, frequency and flexure amplitude on the propulsion performance of the rigid and flexible tuna-tails are investigated. Computational results reveal that a pair of leading edge vortices develop along the tail surface as it undergoes an oscillating motion. The propulsive efficiency has a strong correlation with various locomotive parameters. Peak propulsive efficiency can be obtained by adjusting these parameters. Particularly, when input power coefficient is less than 2.8, the rigid tail generates larger thrust force and higher propulsive efficiency than flexible tail. However, when input power coefficient is larger than 2.8, flexible tail is superior to rigid tail.

Keywords: tuna-tail, RANS, propulsion mechanism, hydrodynamic characteristics, viscous flow-fields

Copyright © 2011, Jilin University. Published by Elsevier Limited and Science Press. All rights reserved.

doi: 10.1016/S1672-6529(11)60046-2

1 Introduction

In recent years, the bio-inspired propulsion system imitating the way which aquatic animals adopt to propel them forward has been widely applied in Autonomous Underwater Vehicle (AUV) design. Among various propulsion mechanisms such as using body undulation, oscillating pectoral fins and caudal fin, AUV with biomimetic caudal fin becomes the most popular propulsion system due to its relatively simple design while with high propulsion efficiency. The rapid development of AUV industry has inspired the fundamental fluid mechanics research on the flow mechanism of oscillating caudal fins such as tuna or dolphin utilize for their propulsion. Many researches have been done for two-dimensional flapping foil and three-dimensional flapping wing to investigate the effect of oscillating frequency, amplitude and phase difference between pitching and heaving motions on the propulsion thrust and efficiency. For three-dimensional flapping wing, most of studies are focused on the rectangular wing with cross-sectional shape of NACA series. Limited researches have been carried out on the hydrodynamic performance investigation for lunate-tail[1–5]. However, tuna, dolphin and shark exhibit excellent hydrodynamic performance with high cruising speed, efficiency and low noise with lunate-tails. The research on such type of tail is therefore important for AUV design by shedding the flow physics insight.

In 1970, Lighthill[1] investigated the caudal fin as a flat wing with two-dimensional foil theory and this method was further extended to three-dimensional wing by Chopra and Kambe[2]. Wu[3] studied swimming propulsion problems by utilizing potential flow theory. Karpouzian *et al*.[4] applied lifting line theory to various shapes and morphological features of lunate-tail. Their investigation on the propulsion thrust and efficiency showed that the crescent-moon shape fin at moderate sweep angles achieved better hydrodynamic performance than V-shape tail. A potential flow based time

Corresponding author: Liang Yang
E-mail: yangliang@hrbeu.edu.cn

domain panel method was used by Liu and Bose[5,6] to examine the performance of a lunate and rectangular foil with a large amplitude unsteady motion. They found that within a range of reduced frequencies between 0.5 and 1.0, the lunate-tail obtained a higher propulsive efficiency than rectangular foil. In terms of thrust coefficient, lunate planform achieved a lower thrust coefficient at a heavy load condition and a higher thrust at a medium load condition.

Compared to large number of researches on the propulsion performance of rigid fin, the studies on flexible fin are few. Miao and Ho[7] investigated a flexible foil in plunging unsteady motion with various combinations of oscillating frequency and Reynolds number. Their simulation results show that propulsion efficiency is enhanced with flexure amplitude of 0.3 of the chord length. The effect of bending flexibility on the unsteady aerodynamics performance of a flexible wing was studied by Qi *et al*.[8] using Lattice Boltzmann Flexible Particle Method (LBFPM). They found that for a combined plunge and pitch motion, flexibility initially increases the lift and drag forces and then dramatically reduces these two forces when the flexibility becomes excessively large. Wang *et al*.[9] studied two-dimensional and three-dimensional flexible fins with heaving and pitching motions using commercial CFD package FLUENT. Particularly, investigations were focused on the influence of chord-wise deflexion length on the propulsion characteristics. Tay and Lim[10] studied the effect of chord-wise flexing on the lift, thrust and propulsive efficiency of three types of airfoils with heaving motion. The flexibility is reflected by varying the flexing center location, standard two-sided flexing and single-sided flexing. Their simulation results show that flexing is not always beneficial to the propulsion performance of airfoils. Instead, it depends on the type of flapping configurations. Riggs *et al*.[11] experimentally investigated flexible NACA0012 fins with a stiffness profile mimicking that of a Pumpkinseed Sunfish under a pitching sinusoidal motion. With the measurement of torque, lateral force and static thrust over a series of frequencies and amplitudes, they concluded that the biomimetic fins could obtain 26% greater thrust per watt of input power over rigid fins.

Above researches on the flexible fins have shown that the flexibility of fins plays a significant role in the propulsive performance. However, whether the flexible fins' propulsion thrust and efficiency are enhanced depends on the extent of flexibility and also other kinematic parameters such as oscillating frequency and amplitude. Although some insights are shed from these studies, some deeper investigations on this problem are needed, such as how wake structure relates to the propulsive performance, which has not been fully studied by previous research. In addition, for conventional rotational propeller, the power output per unit of power input is a key criterion to quantify the propeller's performance. However, little research has been done to judge the propulsive performance of biomimetic caudal fin with this parameter.

The aim of the present paper is to study the propulsive mechanisms of rigid and flexible oscillating tuna-tails by numerical modeling. Different from previous investigations, attention will be focused not only on the tail hydrodynamic performance, but also on the corresponding wake vorticity structure. The comparison of the hydrodynamic thrust, efficiency and more important the output power between rigid and flexible fins will be performed based on the same input power. The main three-dimensional vortex difference associated with rigid and flexible tails will be analyzed.

2 Calculation model

For a lunate caudal fin, we adopt a coordinate system shown in Fig. 1. Assume tuna swims at a constant speed V_0, the movement of its caudal fin is composed of swaying in z direction and yawing around y-axis. The motion equations of caudal fin are defined as:

$$\begin{cases} z(t) = A_z \sin(2\pi ft) \\ \theta(t) = \theta_0 \sin(2\pi ft + \varphi_0) \end{cases}. \tag{1}$$

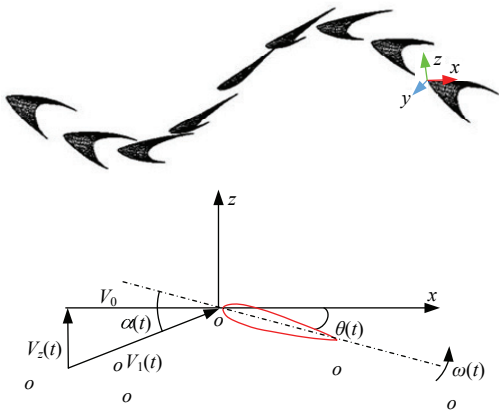

Fig. 1 Coordinate system and notation of caudal fin.

The corresponding swaying velocity $V_z(t)$ and yawing angle velocity $\omega(t)$ are expressed as:

$$\begin{cases} V_z(t) = 2\pi f A_z \cos(2\pi f t) \\ \omega(t) = 2\pi f \theta_0 \cos(2\pi f t + \varphi_0) \end{cases}, \tag{2}$$

where A_z and θ_0 are the amplitudes of swaying and yawing respectively; f is the oscillating frequency and φ_0 is the phase difference between swaying and yawing.

The coordinate system is fixed on the caudal fin, which moves forward together with the tail. The absolute velocity of any point on the tail surface is expressed as:

$$\vec{V}_p(x,y,z,t) = \vec{V}_0 + \vec{V}_z(t) + \vec{V}_\theta(x,y,z,t), \tag{3}$$

where $\vec{V}_\theta$ is the yawing velocity of the point on the surface of the tail.

The thrust coefficient C_x, lateral force coefficient C_z, pressure coefficient C_p and the moment coefficient C_{my} about y-axis of the tail are determined as follows:

$$\begin{cases} C_x = \iint_{S_b} \dfrac{\boldsymbol{p}_n}{1/2\rho C_0 B V_0^2} \boldsymbol{n}_x \mathrm{d}s \\ C_z = \iint_{S_b} \dfrac{\boldsymbol{p}_n}{1/2\rho C_0 B V_0^2} \boldsymbol{n}_y \mathrm{d}s \\ C_p = \iint_{S_b} \dfrac{\boldsymbol{p}}{1/2\rho V_0^2 S} \boldsymbol{n} \mathrm{d}s \\ C_{my} = \iint_{S_b} \dfrac{\boldsymbol{p}_n}{1/2\rho C_0^2 B V_0^2} (x\boldsymbol{n}_z - y\boldsymbol{n}_x) \mathrm{d}s \end{cases}, \tag{4}$$

where, $\boldsymbol{n}_x$, $\boldsymbol{n}_y$, $\boldsymbol{n}_z$ are normal unit vectors of the tail surface, $\boldsymbol{p}_n$ and $\boldsymbol{p}$ are total force and pressure force on the panel ds respectively. The propulsive efficiency of caudal fin is defined as:

$$\eta = \frac{\dfrac{1}{T}\int_0^T F_x \mathrm{d}t \cdot V_0}{\dfrac{1}{T}\left(\int_{z(0)}^{z(T)} F_z \mathrm{d}z + \int_{\theta(0)}^{\theta(T)} M_y \mathrm{d}\theta\right)}, \tag{5}$$

where T is the oscillating time period. Assume that C_{xm} is the time-averaged value of the thrust coefficient. Eq (5) can be nondimensionalized by $\frac{1}{2}\rho V_0^3 S$, then we obtain

$$\eta = \frac{C_{xm}}{\dfrac{1}{V_0 T} \cdot \left(\int_{z(0)}^{z(T)} C_z \mathrm{d}z + \int_{\theta(0)}^{\theta(T)} C_{my} \cdot C_0 \mathrm{d}\theta\right)}, \tag{6}$$

or

$$\eta = \frac{C_{xm}}{(K_P \cdot f)/V_0}. \tag{7}$$

In Eq. (7), the numerator can also be defined as *output power coefficient* and the denominator can be defined as *input power coefficient*, where the consumed power coefficient K_P is defined as:

$$K_P = \int_{z(0)}^{z(T)} C_z \mathrm{d}z + \int_{\theta(0)}^{\theta(T)} C_0 C_{my} \mathrm{d}\theta. \tag{8}$$

3 Numerical methodology

In this study, the unsteady viscous flow-field around the rigid and flexible tuna-tails is simulated by solving Navier–Stokes equations. The simulations are performed using the commercial CFD package Fluent 6.3 based on the control-volume method. The viscous model in all runs is based on k–ω SST model. The coupling between the pressure and the velocity is achieved by PISO algorithm. The time accuracy is improved by utilizing the first order implicit method. The residual smoothing approach is also applied to accelerate the convergence of solutions within each physical time step.

3.1 Grid generation

To generate the proper mesh topology for the accurate hydrodynamic prediction of flapping tail is an essential part of CFD process. Tuncer and Kaya[12] used overset grids to obtain good solutions for a single rigid flapping foil. However, the latest developed dynamic mesh technique in FLUENT proves a viable alternative for simulating the unsteady flow field induced by a flapping foil with various modes. Fewer restrictions exist on the implementation of the dynamic mesh technique in a computational domain consisting of triangular cells.

In order to accurately simulate the developing boundary layer flow on the flapping foil, the current study adopts the unstructured mesh. This strategy is based on the earlier study of Guo *et al*.[13], where the dynamic mesh technique was employed to model the flapping motion of tails using ‘‘Spring-based smoothing” method. Additionally, the overall computational domain is divided into kernel and non-kernel areas. In the kernel areas, the size of the cells at least should be 1/20 or 1/30 of the characteristic chord length of tail.

Fig. 2 shows the mesh around the tail. Following grid refinement studies, the final computational domain is composed of 1005260 unstructured cells, which are used to encompass the entire tail.

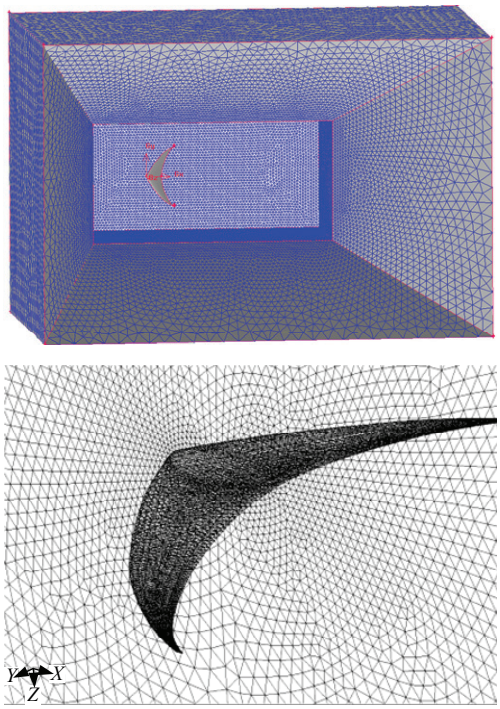

Fig. 2 Grid system around the tail.

3.2 Boundary conditions

For viscous flow considered here, the instantaneous flow velocity on the tail surface must be equal to the local surface velocity described by the swaying and yawing motions of the tail. A no-slip boundary condition is therefore imposed on the surface, and the tail motion defined by Eq. (1) is implemented by UDF program[14]. Inflow and outflow boundary conditions are imposed on the left and right bounds of computational domain. In general, it is found that a quasi-steady solution is obtained after four to six oscillating cycles. The solution is considered to be convergent when the difference of computed thrust coefficient values in successive oscillating cycles is less than 5%.

3.3 Validation

To validate the numerical approach, the flow across a rigid trapezoidal wing is considered. Both steady and oscillating cases are tested. The section of wing is NACA0018 and the aspect ratio of wing is taken as 1.0, swept-back angle $\varphi = 10^\circ$ and root-tip ratio $b_t/b_r = 0.62$. The oscillating period is $T = 3.699$ s and pitching amplitude $\theta = 25^\circ$. The geometric parameters of trapezium wing are shown in Fig. 3a. Figs. 3b and 3c show the lift and drag coefficients variation with the angle of attack for steady and oscillating wings, along with the experimental measurement. Generally, the present calculated results are in good agreement with the experimental results presented in Ref. [15]. It appears that the fin shaft could be one of the reasons for the difference between the computed and measured coefficients in Figs. 3b and 3c.

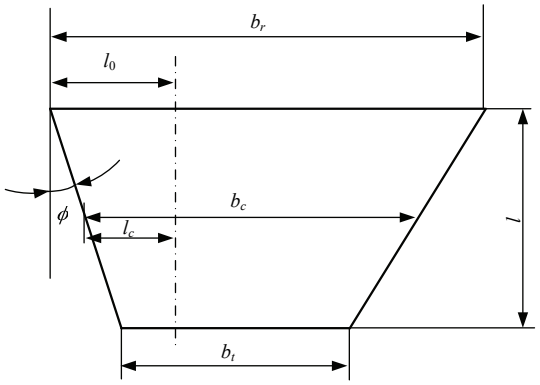

(a) Geometric parameter of trapezium wing

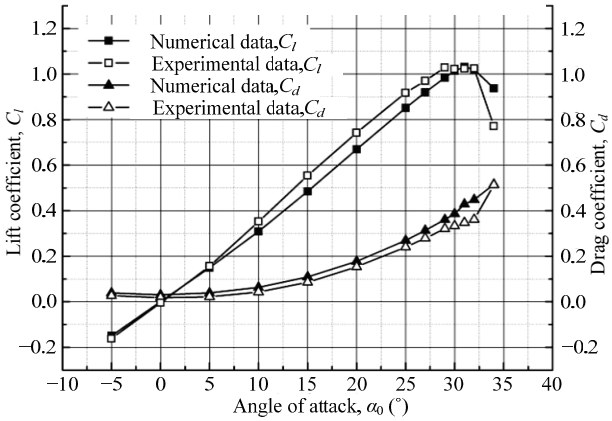

(b) Steady

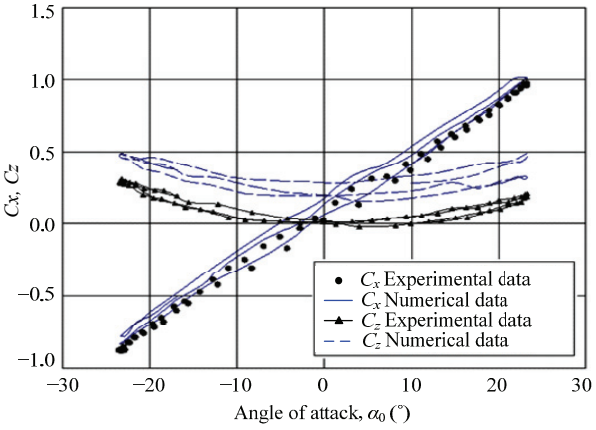

(c) Unsteady

Fig. 3 Hydrodynamic performance of trapezium wing.

4 Results and discussion

4.1 Rigid tuna-tail

Investigation on an oscillating rigid tuna-tail with NACA0028 shape is conducted at swaying amplitude $A_z = 0.4C_0$, yawing amplitude $\theta_0 = 20^\circ$, and swimming speed $V_0 = 7C_0$ m·s^{-1}, where C_0 is the chord length, defined as the vertical distance from leading edge point to interconnecting line of two tail tips, and is equal to 0.312 m. The phase angle between swaying and yawing is $\varphi_0 = 90^\circ$. The oscillating period is set to 0.5 seconds and composed of 400 time steps. The Reynolds number Re is equal to 6.8×10^5.

4.1.1 Instantaneous hydrodynamic performance

In Fig. 4a, the temporal evolutions of swaying position $z(t)$, yawing angle $\theta(t)$ and resulting angle of attack $\alpha(t)$ are plotted. The development of lateral force coefficient, moment coefficient and thrust coefficient are shown in Fig. 4b. As seen in Fig. 4b, although the amplitudes of lateral force coefficient and moment coefficient are larger than that of thrust coefficient, the time-averaged C_z, C_{my} approach to zero, and a positive averaged thrust coefficient is obtained.

Figs. 5a–5i show the instantaneous vortex contour around tail and the pressure contour at the tail surface. The top figures show the vorticity contours in the tuna-tail wake, and the bottom figures show the pressure and the vortex distribution on the slices located at the middle of tail and perpendicular to the flow direction. The phase angle is π/2 between swaying and yawing, thus the rigid tail moves to the left-most position at time $t+T/4$, and the right-most position at time $t+3T/4$. To better analyze the pressure distribution along tail surfaces, Figs. 6 and 7 plot the pressure contour on the left and right surfaces of tuna-tail assuming tuna swims forward from right to left.

At $t = 0$, the first vortex is generated at the trailing edge. With the continuous tail oscillating, this vortex is shed into the wake, and the vortex strength also decreases gradually. Meanwhile, the higher pressure distribution on the left side of the tail moves gradually to a central position along the chord of the tail, and the lower pressure distribution on the right side of the tail also moves gradually to a central position along the chord of the tail. Thrust coefficient, influenced by the variation of

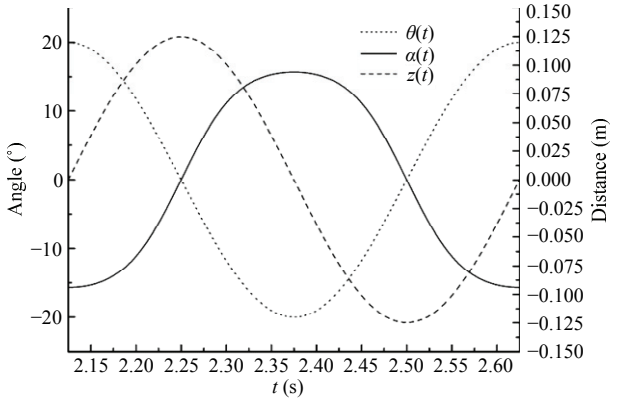

(a) Temporal evolutions of swaying position, yawing angle and resulting angle of attack

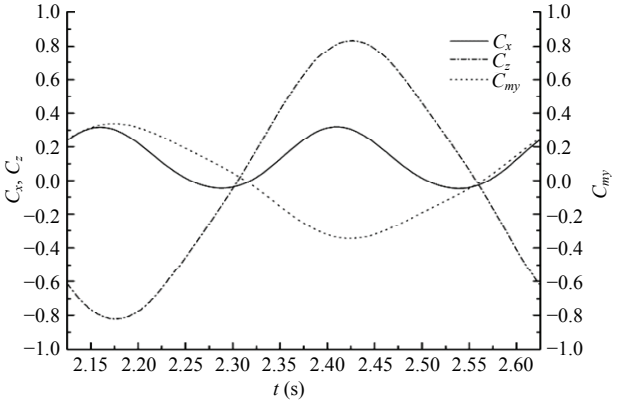

(b) Time dependent thrust force, lateral force and moment coefficients

Fig. 4 Hydrodynamic performance of rigid tuna-tail during one period.

vortex movement and pressure distribution, remains a decreasing trend, until the first vortex sheds from the tail trailing edge. After $t+T/4$, the second vortex moves gradually to a central position along the chord of the rigid tail. The corresponding thrust coefficient increases to the maximum value and then decreases, until the second vortex moves into the wake flow. The difference between the pressure on left and right surfaces results in either an ascending or a descending trend of the thrust coefficient and lateral force coefficient.

From $t+3T/4$ to $t+T$, the third vortex is generated and gradually becomes stronger on the tail surface. The surface pressure distribution reflects the pattern observed during time instants from $t+T/4$ to $t+T/2$, and the thrust coefficient increases again. Thus, in one oscillating cycle, the thrust coefficient undergoes two cyclic variations.

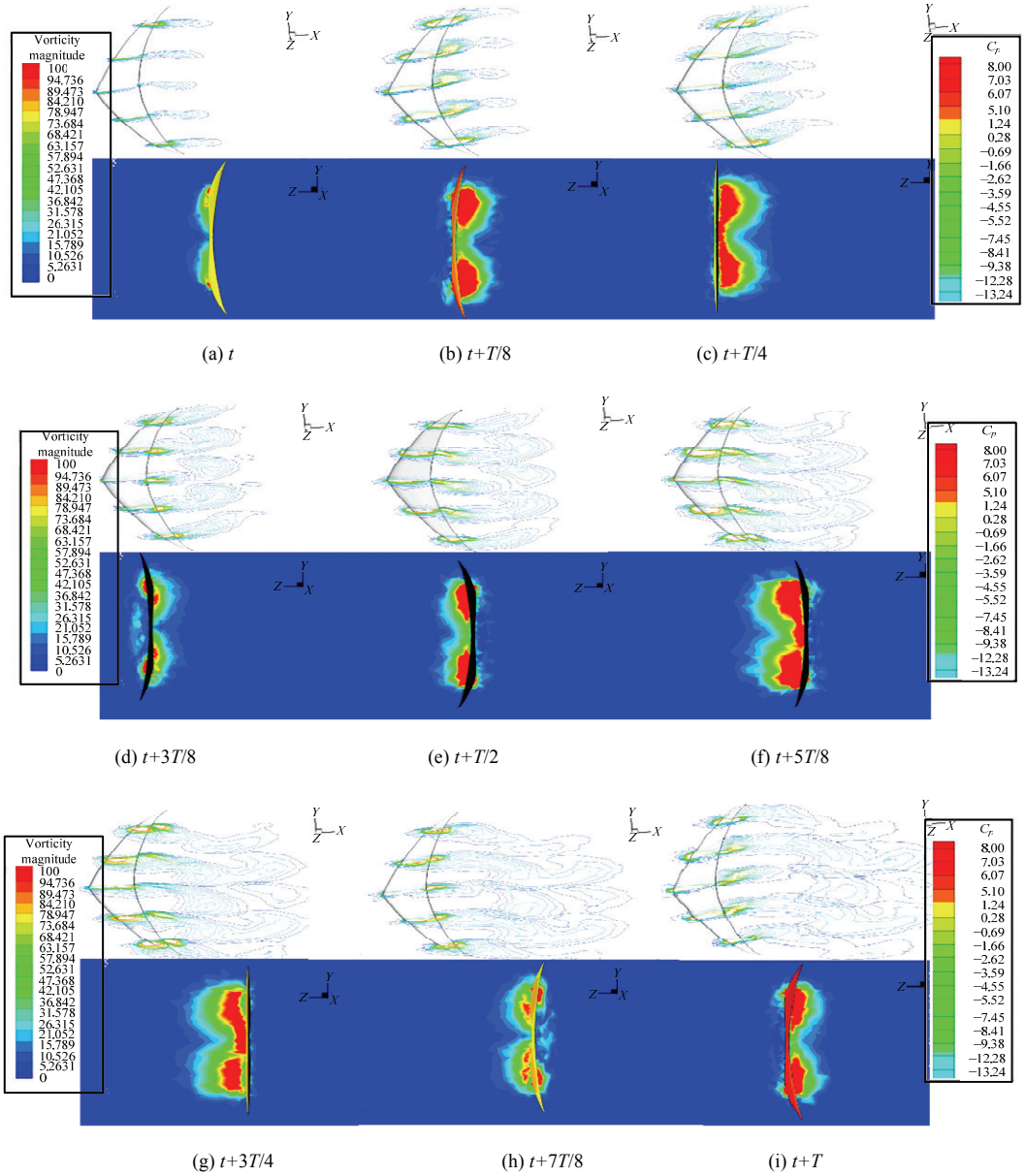

Fig. 5 Instantaneous vorticity contour around tuna-tail and tail surface pressure contour.

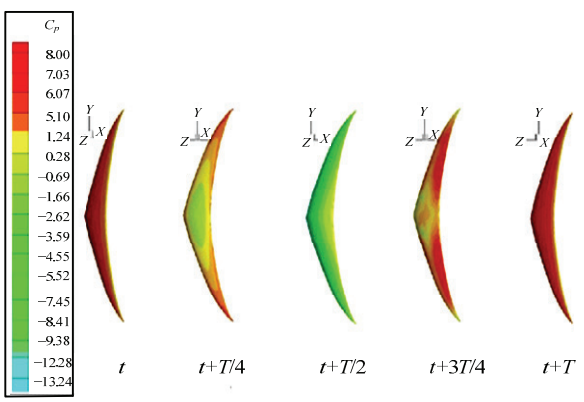

Fig. 6 Pressure distribution on the left surface of tail (viewed from downstream).

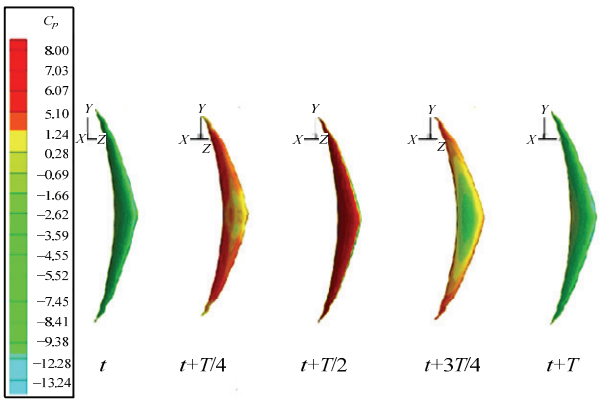

Fig. 7 Pressure distribution on the right surface of tail (viewed from downstream).

The vorticity contours in the tail wake at three slices perpendicular to y axis are shown in Fig. 8. In the middle plane, the vortices do not interact with each other. However, in the planes near to two tips, vortices begin to merge partially. Additionally, reverse Karman Vortex Street of wake structure can be clearly seen in Fig. 8.

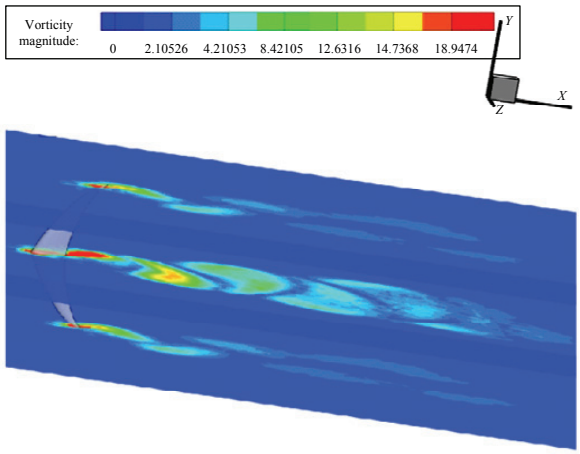

Fig. 8 Vortex pattern visualization in y-slice of wake flow field at t+3T.

4.1.2 Time-mean hydrodynamic performance

In Figs. 9–11, the variations of time-mean input power coefficient, output power coefficient (defined in Eqs. (5–7)) and propulsive efficiency are plotted with respect to the different inflow velocities, yawing angles, swaying amplitudes. Fig. 12 shows the influence of oscillating frequencies for rigid and flexible tuna-tails.

Fig. 9 shows that the input power coefficient and output power coefficient decrease with the increase in inflow velocity at $\theta_0 = 20^\circ$, $A_z = 0.4C_0$, $f = 2.0$ Hz, $\varphi_0 = \pi/2$. However, the variation of propulsive efficiency with inflow velocity is not monotonic. The propulsive efficiency initially increases by 50% as the inflow velocity increases from zero to $V_0 = 7C_0$ m·s^{-1}, then decreases as the velocity increases further from $7C_0$ m·s^{-1}.

Fig. 10 illustrates the influence of the yawing angle on the input, output power coefficients and propulsive efficiency from $\theta_0 = 5^\circ$ to $\theta_0 = 30^\circ$ at $V_0 = 7C_0$ m·s^{-1}, $A_z = 0.4C_0$, $f = 2.0$ Hz, $\varphi_0 = \pi/2$. The peak value of propulsive efficiency can be achieved at $\theta_0 = 20^\circ$.

It is well known that the variation of swaying amplitude also influences the propulsion performance of oscillating tuna-tail. The hydrodynamic characteristics of lunate fin with different swaying amplitudes are shown in Fig. 11 at $V_0 = 7C_0$ m·s^{-1}, $\theta_0 = 20^\circ$, $f = 2.0$ Hz, $\varphi_0 = \pi/2$. It is seen that, with the increases in input and output power coefficients, the propulsive efficiency reaches a maximum value of 82% at $A_z = 0.7C_0$.

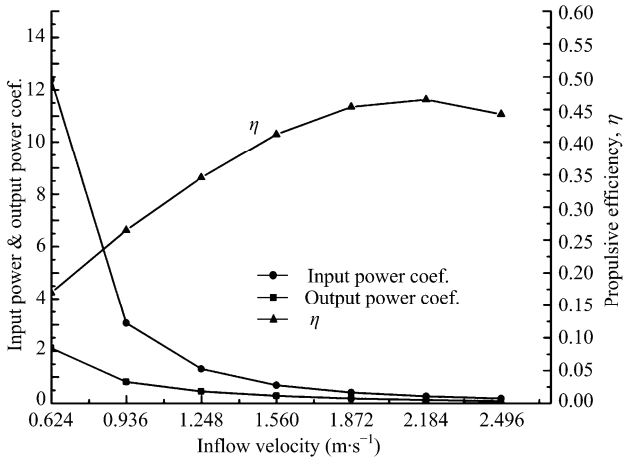

Fig. 9 Input, output power coefficients and propulsive efficiency variation with inflow velocity (rigid tuna-tail).

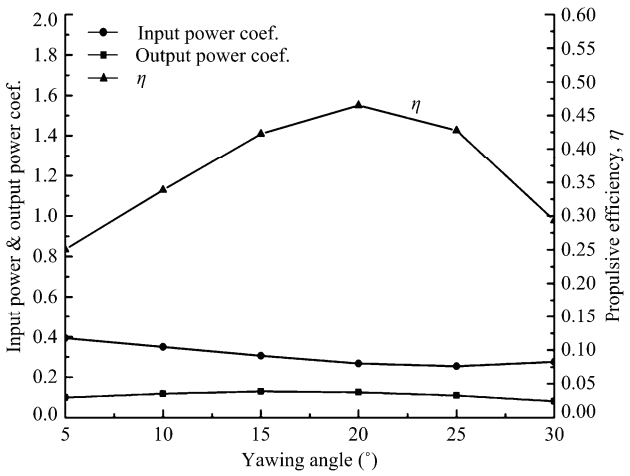

Fig. 10 Input, output power coefficients and propulsive efficiency variation with pitch angle (rigid tuna-tail).

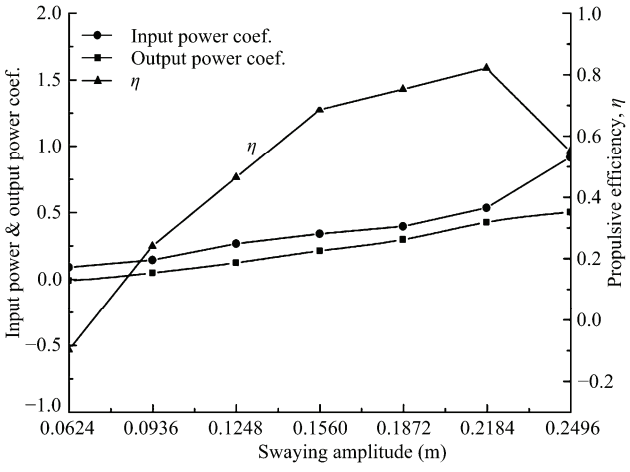

Fig. 11 Input, output power coefficients and propulsive efficiency variation with swaying amplitude (rigid tuna-tail).

The influence of oscillating frequency on the input, output power coefficients and propulsive efficiency is shown in Fig. 12 for rigid and flexible tuna-tails, in which $V_0 = 7C_0$ m·s^{-1}, $\theta_0 = 20^\circ$, $A_z = 0.7C_0$, $\varphi_0 = \pi/2$. For both tails, it is seen that the output power coefficients increase linearly with the oscillating frequency for f >2.0 Hz. However, the input power coefficients increase exponentially with the oscillating frequency, leading to a maximum propulsive efficiency appearing at f = 2.0 Hz for rigid tail. Obviously, this is due to the fact that, to retain the tail at larger oscillating frequency requires larger power input.

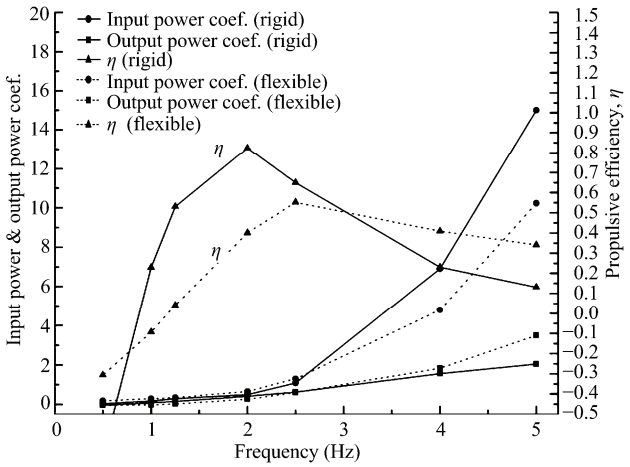

Fig. 12 Input, output power coefficients and propulsive efficiency variation with oscillating frequency (rigid and flexible tuna-tails).

4.2 Flexible tuna-tail

For the flexible tuna-tail studied here, the kinematic profile (swaying and yawing) is assumed to be identical to that of the rigid tuna-tail, while the tail shape deforms at a prescribed flexure. We assume that the tail is a good reflection of a thin wing, therefore, only deformation in z-direction is considered. The deformation profile is simplified and facilitated with the analysis of the effect of flexure amplitude described as

$$z = -\frac{a_0}{C_0}(x - b_0)^2 \cos(\omega t + \psi), \tag{9}$$

where a_0 denotes the flexure amplitude, b_0 denotes the x-coordinate of initial point on the deforming part, and ψ denotes the phase angle of deformation.

For oscillating flexible tuna-tail, the swaying amplitude is fixed as $A_z = 0.7C_0$, the yawing amplitude $\theta_0 = 20^\circ$, the inflow velocity $V_0 = 7C_0$ m·s^{-1}, and the phase angle between swaying and yawing $\varphi_0 = \pi/2$. The flapping frequency f = 4.0 Hz and the deformation phase angle $\psi = \pi/2$.

4.2.1 Instantaneous pressure and vorticity contour

Fig. 13 illustrates the deformation of flexible tail and the pressure contours in one quarter of a cycle.

Fig. 14 shows instantaneous vorticity contour in the tail wake within one cycle. A section located in the middle of tuna-tail and perpendicular to the span direction of caudal fin is drawn. It is seen that, the vortices shed from tail do not interact with each other (see top figures). This is similar to the rigid tail. However, at the trailing edge section, due to the large flexible deformation, the development of separated vortex takes longer time, and the vortices in the wake merge with each other (see bottom figures).

4.2.2 Time-mean propulsion efficiency

To compare the effect of flexibility on the propulsion efficiency of rigid and flexible tails, the conventional rotational propeller concept is adopted here. We can plot propulsion efficiency as function of input power coefficient for rigid and flexible tails as shown in Fig. 15. It is clearly seen that, rigid tail obtains a higher peak efficiency than flexible tail at input power coefficient around 0.5. However, flexible tail covers a wider range of large efficiency than rigid tail. From Fig. 15, we also find that, the propulsive efficiency of rigid tail is higher than that of flexible tail for input power coefficient less than 2.8. The propulsive efficiency of flexible tail is higher than that of rigid tail for input power coefficient larger than 2.8.

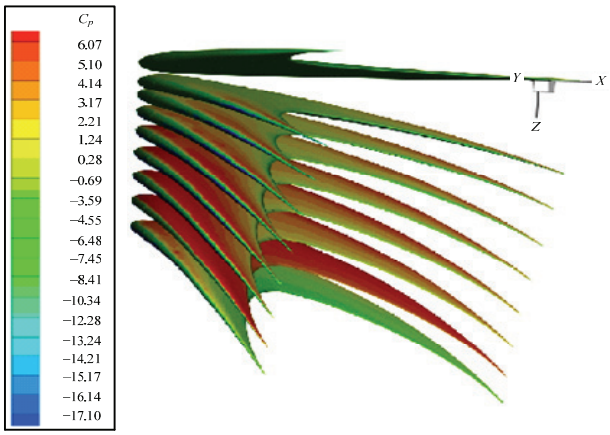

Fig. 13 Profiles of flexible tail and the corresponding pressure contours in $T/4$.

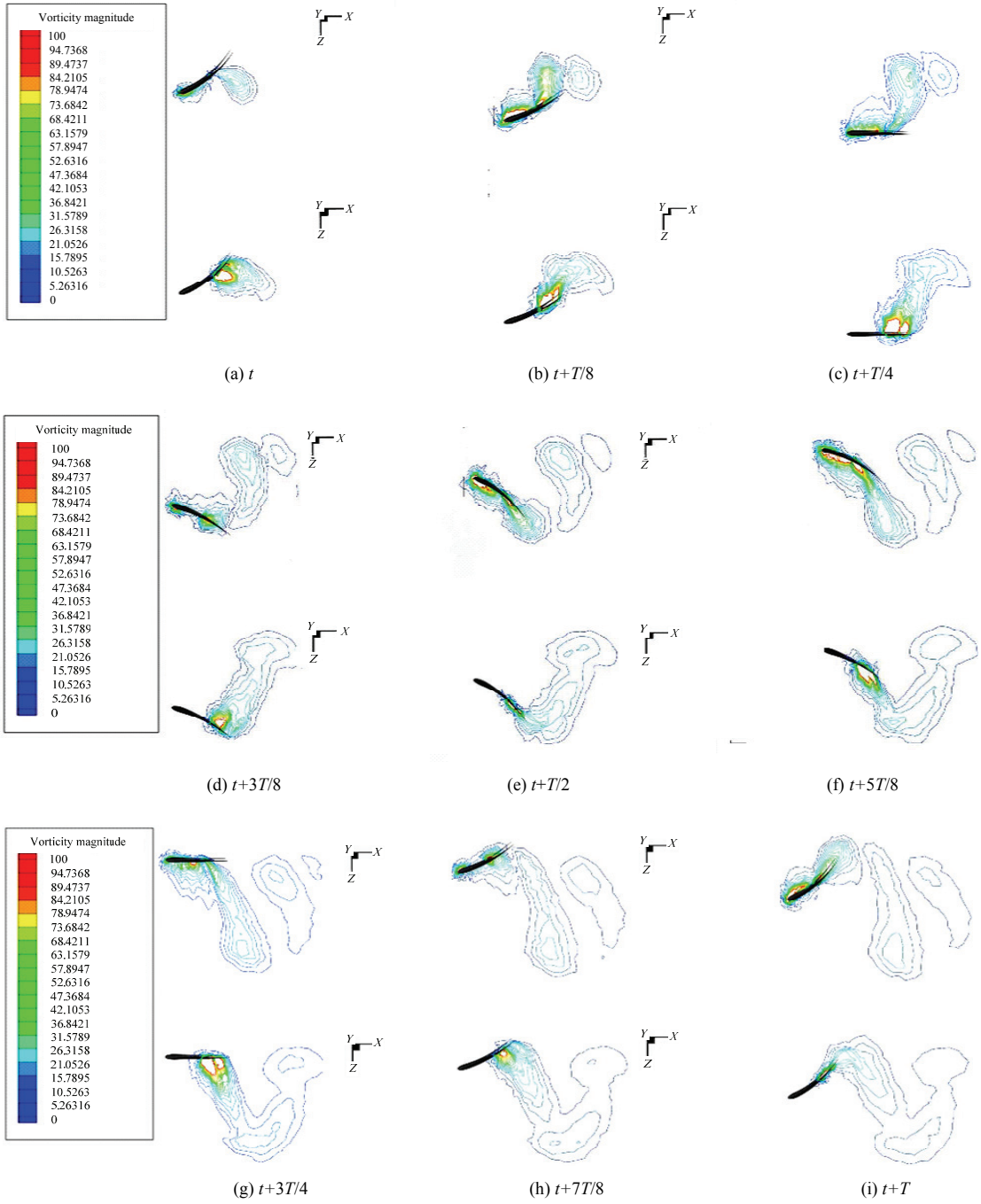

Fig. 14 Vorticity contour in the flexible tuna-tail wake at the middle section.

Look back at Fig. 12, it is interesting to note that to reach the same input power coefficient of 4.8, the rigid tail oscillates at f = 3.6 Hz and the flexible tail oscillates at f = 4.0 Hz. The flexible tail time-mean thrust coefficient C_{xm}, which is also named as output power coefficient, is larger than that of the rigid tail. This can be clearly reflected from instantaneous thrust, lateral force and moment coefficients plot in Fig. 16. In fact, we can see from Fig. 16, the integral area of instant thrust coefficient of flexible tail, which is time-mean thrust coefficient C_{xm} in Fig. 12, is larger than that of rigid tail. This leads to the above observation, i.e. at the same input power coefficient of 4.8, the oscillating frequency of flexible tail must be higher than that of rigid tail if other conditions are the same, such as swimming speed, yawing angle and swaying amplitude. However, flexible tail can achieve a larger thrust force than rigid tail.

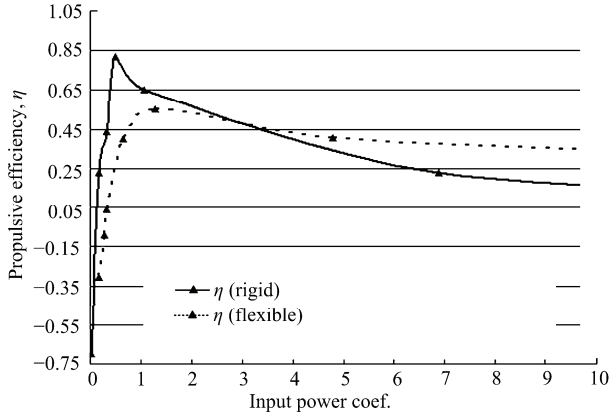

Fig. 15 Propulsive efficiency variation with input power coefficient (comparison between rigid and flexible tails).

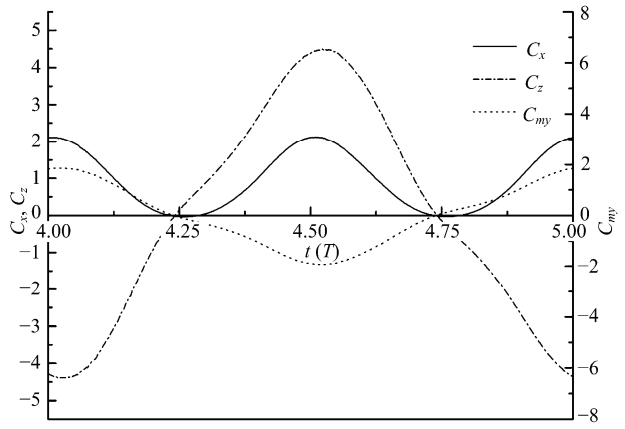

(a) Rigid tail (f = 3.6 Hz)

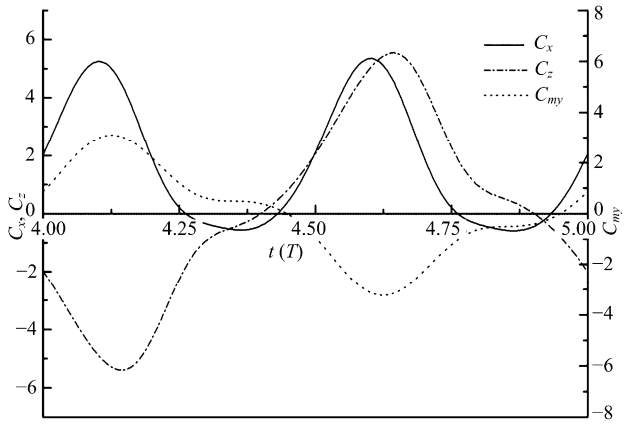

(b) Flexible tail (f = 4.0 Hz)

Fig. 16 Time dependent thrust force, and lateral force and moment coefficients.

4.2.3 Possible flow mechanism

To demonstrate the possible flow mechanism for different behaviors of rigid and flexible tails as discussed above, we plot the vortices shedding for rigid and flexible tails at two time instants t+3T/10 and t+8T/10 and input power coefficient of 4.8 in Fig. 17. At each instant, the top figures show the contours of the vorticity magnitude for rigid tail-shed wake at three different sections, i.e. 1/4-chord length, mid-chord length and trailing edge of tail. Bottom figures show the contours of the vorticity magnitude for flexible tail-shed wake.

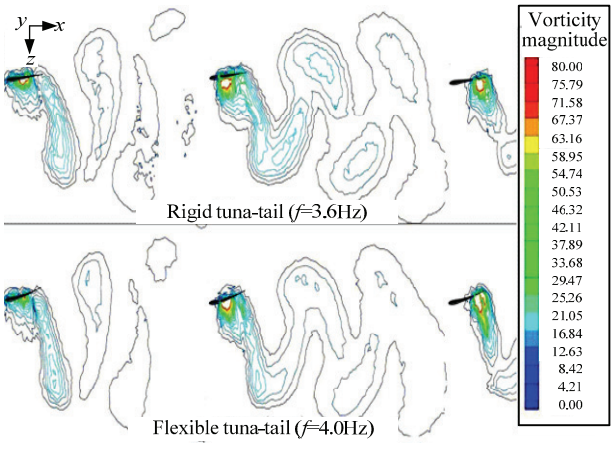

(a) t+3T/10

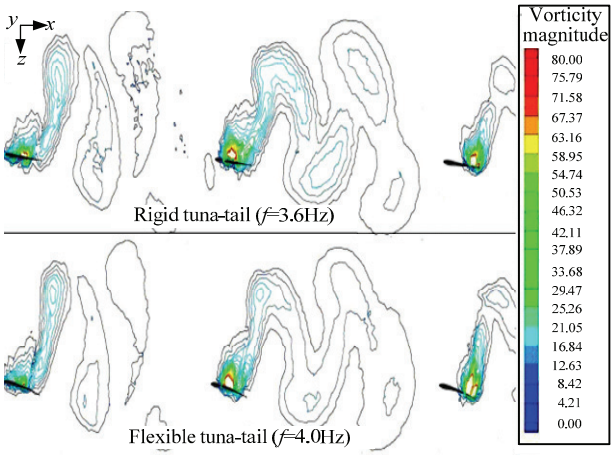

(b) t+8T/10

Fig. 17 Comparison of shedding vortices at the input power coefficient of 4.8 for rigid and flexible tails.

It is seen that, at t+3T/10 instant, the first vortex is released from the tail surface. The vorticity magnitudes of rigid tail are larger than those of flexible tail at 1/4-chord length and mid-chord length sections. At trailing edge of tail, although rigid tail has smaller vorticity magnitude than flexible one, due to its relative small value, the influence on the overall thrust force and propulsion efficiency can be neglected.

At t+8T/10 instant, the second vortex is released from tail surface. Similar observation is obtained as time

instant of t+3T/10. Since the majority of energy dissipates into the wake, partial energy converts to thrust force, more vigorous wake structure thus indicates large energy loss. This is why the energy loss of rigid tail is larger than that of flexible tail, while flexible tail has larger thrust force than rigid tail.

4.2.4 Flexure amplitude effect

Fig. 18 illustrates the flexure amplitude effect on the input, output power coefficients and propulsive efficiency at $A_z = 0.7C_0$, $\theta_0 = 20^\circ$, $V_0 = 7C_0$, $\varphi_0 = \pi/2$, $\psi = \pi/2$, and $f = 2.5$ Hz. It is seen that propulsive efficiency initially increases as tuna tail becomes more flexible until the flexure amplitude reaches 0.4. The propulsive efficiency then decreases as the flexure amplitude increases further.

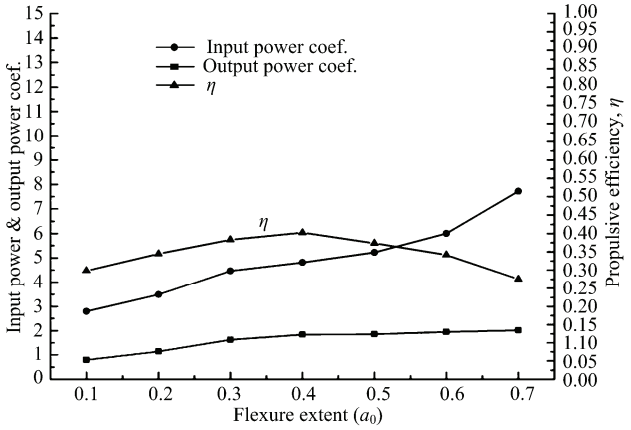

Fig. 18 Flexure extent analysis for flexible tail.

5 Conclusion

The following conclusions can be drawn based on the above discussions:

(a) For an oscillating tuna-tail, tail surface pressure distributions and vortices shedding structure from tail have direct relationships with the thrust coefficient, lateral force coefficient and moment coefficient.

(b) The input, output power coefficients and propulsive efficiency vary with in-coming velocities, yawing angles, swaying amplitudes and oscillating frequency. Maximum propulsion efficiency is obtained depending on various combination of above parameters.

(c) The input power coefficient has strong link with in-coming velocity, swaying amplitude, yawing angle and oscillating frequency. When the hydrodynamic load on the tail is less, for example, input power coefficient is less than 2.8, rigid tail generates larger thrust force and higher propulsive efficiency than flexible tail at higher oscillating frequency. However, when the hydrodynamic load on the tail is large (input power coefficient is larger than 2.8), the flexible tail has better performance than rigid tail in terms of thrust force and propulsion efficiency.

(d) To achieve an optimal propulsive efficiency, the present result implies that flexure amplitude should be controlled to be 0.4 for the chord-wise flexible tuna-tail.

References

[1] Lighthill M J. Aquatic animal propulsion of high hydro mechanical efficiency. *Journal of Fluid Mechanics*, 1970, **44**, 265–301.

[2] Chopra M G, Kambe T. Hydromechanics of lunate-tail swimming propulsion Part II. *Journal of Fluid Mechanics*, 1977, **79**, 49–69.

[3] Wu T Y. Hydrodynamics of swimming propulsion, Part I. Swimming of a two-dimensional flexible plate at variable forward speeds in an inviscid fluid. *Journal of Fluid Mechanics*, 1971, **46**, 337–355.

[4] Karpouzian G, Spedding G R, Cheng H K. Lunate-tail swimming propulsion Part II. Performance analysis. *Journal of Fluid Mechanics*, 1990, **210**, 329–351.

[5] Liu P, Bose N. Propulsive performance of three naturally occurring oscillating propeller platforms. *Ocean Engineering*, 1993, **20**, 57–75.

[6] Liu P, Bose N. Hydrodynamic characteristics of a lunate shape oscillating propulsor. *Ocean Engineering*, 1999, **26**, 519–530.

[7] Miao J M, Ho M H. Effect of flexure on aerodynamic propulsive efficiency of flapping flexible airfoil. *Journal of Fluids and Structures*, 2005, **11**, 1–19.

[8] Qi D W, Liu Y M, Wei S, Hikaru A. Simulation of dynamics of plunge and pitch of a three-dimensional flexible wing in a low Reynolds number flow. *Physics of Fluids*, 2010, **22**, 091901-091901–20.

[9] Wang Z D, Chen P, Zhang X Q. Wake vortex structure characteristics of a flexible oscillating fin. *Journal of Bionic Engineering*, 2008, **5**, 49–54.

[10] Tay W B, Lim K B. Numerical analysis of active chord-wise flexibility on the performance of non-symmetrical flapping airfoils. *Journal of Fluids and Structures*, 2010, **26**, 74–91.

[11] Riggs P, Bower A, Vincent J. Advantages of a biomimetic stiffness profile in pitching flexible fin propulsion. *Journal of Bionic Engineering*, 2010, **7**, 113–119.

[12] Tuncer I H, Kaya M. Thrust generation caused by flapping

airfoils in a biplane configuration. *Journal of Aircraft*, 2003, **40**, 509–515.

[13] Guo Z, Liu J, Qu Z. Realization of dynamic mesh in 2D unstructured mesh. *The* 10*th National Conference of Computational Fluid Dynamic*, Mianyang, China, 2000, 360–364. (in Chinese)

[14] Fluent Inc. FLUENT User Defined Function Manual, 2008.

[15] Tang Z M, Zhao X D. Collection of Illustrative Plates of Hydrodynamic Performance of Stabilizing Fin, Harbin Engineering University Press, Harbin, China, 2004. (in Chinese)